

Development and Control of a Low-Cost Cart-Pendulum Educational Platform

Kyriakos Mouratis, John Fasoulas and Michael Sfakiotakis

Control Systems and Robotics Laboratory

School of Applied Sciences

Technological Educational Institute (T.E.I.) of Crete

Heraklion, Crete 71500, Greece

{kmouratis, jfasoulas, msfak}@staff.teicrete.gr

Abstract—This paper presents the design and control of a low cost cart-pendulum platform, developed for educational purposes. The cart-pendulum is one of the most popular laboratory experiments for teaching and demonstrating underactuated mechanical systems and non-linear control methods, but the cost of commercially available units is typically quite high. Our implementation was built around a linear slide mechanism, salvaged from an old dot-matrix printer, which employs cable transmission to actuate the cart via a DC-motor, driven by a current-control servo amplifier. The platform is outfitted with high-precision optical encoders to measure the pendulum’s angle and the cart’s position. Following the development of the system’s equations of motion, we present a variety of stabilizing controllers in both the upright (inverted pendulum) and the downward (gantry) configurations. A Rapid Control Prototyping approach, based on the WinCon real-time software extension of Matlab/Simulink, is adopted for implementation of these controllers on the developed platform. The experimental results are in very good agreement with those obtained in simulation from a virtual model of the system, which is supplied as an accompanying student educational tool.

Index Terms—Cart-Pendulum, State-Space Modelling, Pole Placement, LQR, Mechatronics, Robotics

I. INTRODUCTION

The cart-pendulum is a very popular laboratory experiment for teaching and demonstrating a variety of concepts and techniques in control engineering. In its most typical implementation, the system involves a freely-swinging pole (pendulum) whose pivot point is mounted on a cart that can be driven along a horizontal tract. This setup represents an underactuated mechanical system with two degrees of freedom (corresponding to the translation of the cart and the rotation of the pendulum) and one control input (the force applied to the cart). The cart-pendulum exhibits two equilibrium points: one with the pendulum hanging vertically (stable equilibrium) and one with the pendulum upright (unstable equilibrium). This characteristic allows studying control tasks of progressive difficulty, depending on the students’ expertise. For example, operation of the system in the stable configuration emulates a translational gantry crane system, which involves the design of feedback controllers to improve the transient performance by

suppressing intense pendulum oscillations during cart motion. The control task becomes more challenging when balancing the pendulum in its inverted position, whereby linear state feedback regulators are usually employed to reject external disturbances. Of particular interest is also the *swingup* problem, i.e., actively raising the pendulum from its resting equilibrium to the upright position; this task is often accomplished through energy shaping methods. Additional parameters to consider for practical implementations include the finite length of the cart tract, the limitation of the control input that can be applied to the system, the unavailability of velocity measurements, and the effect of friction.

Apart from educational purposes, the cart-pole system has also been employed as a benchmark for testing new control techniques, as well as an analogous system for studying a variety of associated problems such as industrial gantry cranes, two-wheeled personal transportation mechanisms [1], missile guidance, vehicle rollover stabilization [2], human gait and balance [3], and friction compensation methods [4].

A number of companies producing educational control model plants offer cart-pendulum systems [5]–[7], but their cost can be quite high. In the present paper, we describe a low cost implementation of the cart-pendulum system, utilizing the linear slide mechanism from a dot-matrix printer. The platform is outfitted with high resolution incremental encoders and a linear servo amplifier that drives the DC-motor generating the

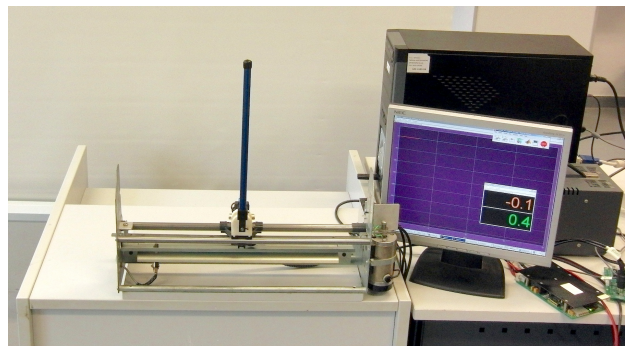


Fig. 1: The developed cart-pendulum system, shown balancing in the inverted pendulum configuration.

The authors are with the Control Systems and Robotics Laboratory, School of Applied Sciences, Technological Educational Institute (T.E.I.) of Crete, Heraklion, Greece. {kmouratis, jfasoulas, msfak}@staff.teicrete.gr

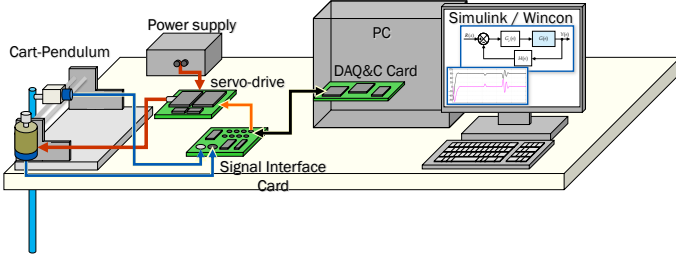


Fig. 2: Overall architecture of the developed cart-pendulum platform.

cart actuation force. Control algorithms are deployed using a Rapid Control Prototyping system based on the WinCon real-time software extension of Matlab/Simulink. A virtual model of the physical platform, which integrates the system's full nonlinear motion equations with a visualization module, is provided as an accompanying educational tool for students.

Section II describes the design and hardware implementation of the physical cart-pendulum platform, whose dynamic model is presented in Section III. Based on this model, stabilizing controllers for the system's two main configurations are designed in Section IV, while the associated experimental results are presented in Section V. Finally, conclusions and suggestions for further work are provided in Section VI.

II. CART-PENDULUM PLATFORM

A schematic overview of the complete cart-pendulum platform, developed for educational and research and purposes, is shown in Fig. 2. The platform consists of the cart and pendulum mechanism, a power supply unit, a servo-drive amplifier, a signal interface card and a PC equipped with a data acquisition and control board (DAQ&C).

The cart-pendulum was built around a linear slide mechanism, salvaged from an old dot-matrix printer (*Texas Instruments OMNI-800*). The linear slide employs a cable transmission, driven by a DC-motor (*IMC 151-20-1*) with an embedded incremental encoder (see Fig. 3), that is used to track the position of the cart with a resolution of 0.0526 mm. A custom base, fabricated in ABSplus material with a 3d-printer, was designed for mounting on the carriage the swivelling pole (an aluminium rod) via dual ball bearings, using an 1024 cpr incremental encoder to measure its angular displacement. The

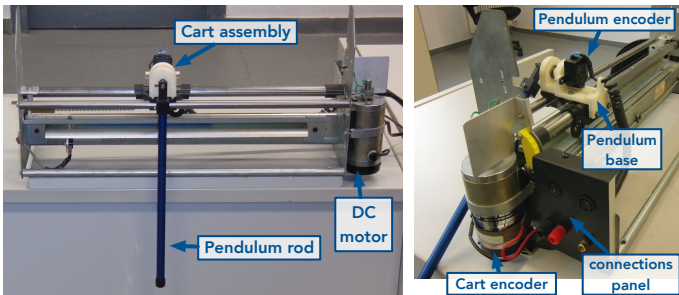


Fig. 3: Details of the cart-pendulum platform.

setup also includes a terminal switch on one end of the linear slide, used as a reference point for the cart position measurement over the 30 cm track length. A linear servo amplifier (*Faulhaber LC3002*), powered by a 24 V supply and operated in current control mode, drives the motor with the desired torque, specified through a ± 10 V voltage signal v_a that is generated by a 12-bit analogue output channel of the employed DAQ&C board (*National Instruments NI-6024E*).

In our setup, the controllers are deployed as Simulink models running under the WinCon real-time software extension, which allows for automatic code generation from a block diagram description of the controller, as well as high sampling rates to limit performance degradation due to discretization. Other similar Rapid Control Prototyping (RCP) schemes can also be implemented, based on, e.g., Simulink's Real Time Windows Target or LabView's Real-Time module. The platform can also be readily interfaced with low cost embedded control units, such as the one described in [8].

III. MODELLING

A. Dynamic equations of motion

In developing a dynamic model for the cart-pendulum system, we consider a rigid homogeneous rod (pendulum) attached by a passive revolute joint to a cart that slides on a horizontal track, initially ignoring the cable/pulley transmission system and the motor dynamics (Fig. 4). Denoting as F the actuating force applied to the cart, the nonlinear equations that describe the dynamics of the system may be derived through a Lagrangian approach as:

$$\begin{aligned} & ((m_c + m_p) I_p + m_c m_p \ell^2 + m_p^2 \ell^2 \sin^2 \theta) \ddot{x}_c = \\ & (I_p + m_p \ell^2) (F - F_{fr,c}(\dot{x}_c)) + m_p^2 \ell^2 g \sin \theta \cos \theta \\ & + (m_p^2 \ell^3 + I_p m_p \ell) \dot{\theta}^2 \sin \theta + m_p \ell \cos \theta F_{fr,p}(\dot{\theta}) \end{aligned} \quad (1)$$

and

$$\begin{aligned} & ((m_c + m_p) I_p + m_c m_p \ell^2 + m_p^2 \ell^2 \sin^2 \theta) \ddot{\theta} = \\ & - m_p \ell \cos \theta (F - F_{fr,c}(\dot{x}_c)) - (m_c + m_p) F_{fr,p}(\dot{\theta}) \\ & - m_p^2 \ell^2 \dot{\theta}^2 \cos \theta \sin \theta - g (m_c + m_p) m_p \ell \sin \theta \end{aligned} \quad (2)$$

Here, m_c is the effective mass of the cart, m_p is the mass of the pendulum rod, g the gravitational constant, ℓ the half length of the rod, $I_p = m_p \ell^2 / 3$ the pendulum's moment of inertia with respect to its center of mass, x_c the position of the cart, and θ the angle of the pendulum. In addition, $F_{fr,p}(\dot{\theta})$ and $F_{fr,c}(\dot{x}_c)$ denote the friction of the pendulum and the cart respectively, described as a function of the respective velocity v using the following generic model:

$$F_{fr}(v) = \left(F_c + (F_{brk} - F_c) e^{(-c_v |v|)} \right) \text{sgn}(v) + f_v v \quad (3)$$

where F_c (Coulomb), F_{brk} (stiction), f_v (viscous coefficient) and c_v (Stribeck coefficient) are the friction parameters as defined in [9].

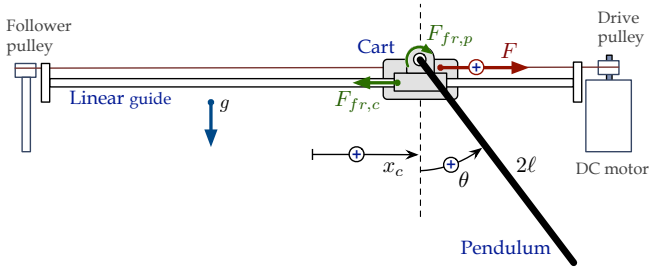


Fig. 4: Cart-pendulum schematic.

B. Cart effective mass

To analyse the effect of the platform's cable drive transmission, we consider the movement along the horizontally oriented linear tract of the cart without the pendulum. A simplified model for the dynamics of this system is:

$$m_0 \ddot{x}_c = F - F_{fr,c}(\dot{x}_c) - \frac{J_{fp}}{r_{fp}^2} \ddot{x}_c - \frac{J_{dp}}{r_{dp}^2} \ddot{x}_c - \frac{J_m}{r_m^2} \ddot{x}_c \quad (4)$$

where m_0 is the mass of the cart, F the force applied to the cart and $F_{fr,c}(\dot{x}_c)$ the total nonlinear friction of the cart. In addition, (r_{dp}, J_{dp}) , (r_{fp}, J_{fp}) and (r_m, J_m) respectively denote the radius and inertia moment of the drive pulley (located on the motor's shaft), the follower pulley, and the motor's armature/shaft. Denoting as m_{fp} , m_{dp} the masses of the pulleys, their moment of inertia can be calculated as:

$$J_{fp} = \frac{1}{2} m_{fp} r_{fp}^2 \quad \text{and} \quad J_{dp} = \frac{1}{2} m_{dp} r_{dp}^2 \quad (5)$$

Rearranging (4), the cart's motion equation can be written as:

$$m_c \ddot{x}_c = F - F_{fr,c}(\dot{x}_c) \quad (6)$$

where m_c is the total effective mass of the cart:

$$m_c = \left(m_0 + \frac{J_{fp}}{r_{fp}^2} + \frac{J_{dp}}{r_{dp}^2} + \frac{J_m}{r_m^2} \right) \quad (7)$$

We may therefore conveniently use m_c as defined above in (1), (2), to account for the cart's increased inertia arising due to the power transmission mechanism of the physical platform.

C. Parameter specification

The numerical values of the system model parameters for the developed platform are summarised in Table I. These were mostly obtained in a straightforward manner, i.e., weighing/measuring the various components to calculate their mass/dimensions, or from the manufacturers' data-sheets. Additional tests were carried out to cross-validate the motor's torque constant K_t (using the in-situ measurement method described in [10]) and the servo-drive amplifier's gain K_a .

The cart friction parameters were identified through a series of tests conducted with the pendulum rod removed from the system, involving a variety of sinusoidal force inputs that were applied to the cart. The acquired experimental data were then fitted to the model of (6), and the resulting friction parameters

TABLE I: Parameters of the system

| Parameter | Symbol | Value | Units in SI |
|----------------------------|----------|------------------------|---------------------|
| cart mass | m_0 | 0.18 | Kg |
| cart effective mass | m_c | 0.8579 | Kg |
| pendulum mass | m_p | 0.125 | Kg |
| pendulum length | 2ℓ | 0.3365 | m |
| pendulum moment of inertia | I_p | 1.2×10^{-3} | Kg · m ² |
| drive pulley radius | r_{dp} | 9.5×10^{-3} | m |
| follower pulley radius | r_{fp} | 9.5×10^{-3} | m |
| drive pulley inertia | J_{dp} | 1.842×10^{-7} | Kg · m ² |
| follower pulley inertia | J_{fp} | 2.072×10^{-7} | Kg · m ² |
| drive pulley mass | m_{dp} | 4.1×10^{-3} | Kg |
| follower pulley mass | m_{fp} | 4.6×10^{-3} | Kg |
| motor torque constant | K_t | 0.075096 | N / A |
| motor shaft radius | r_m | 6.35×10^{-3} | m |
| motor inertia | J_m | 2.716×10^{-5} | Kg · m ² |
| servo-drive amplifier gain | K_a | 0.37811 | A / V |

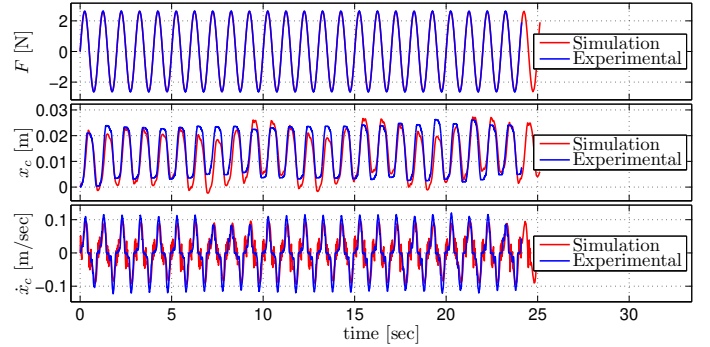


Fig. 5: Cart's nonlinear friction simulated results compared to experimental data. The graphs show the input signal (applied force), and the cart's position and velocity.

are summarized in Table II. Note that, in order to increase the model's fidelity, two different such parameter sets were identified, depending on the cart's motion direction (i.e. the sign of \dot{x}_c). The results presented in Fig. 5 highlight the match between the thus specified model and the experimental data.

In order to calculate the nonlinear friction parameters of the pendulum, the latter was mounted on the cart, and a free

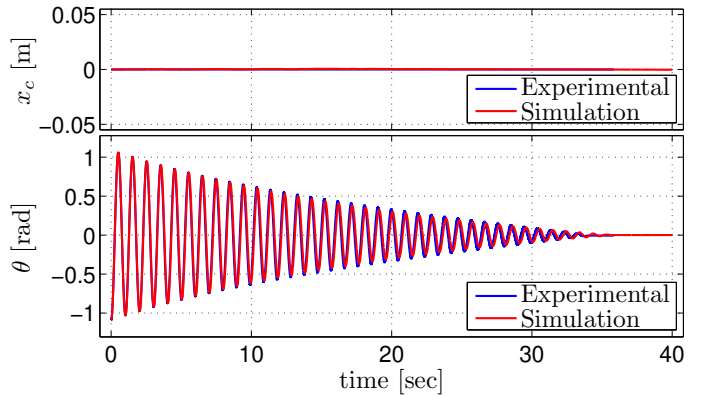


Fig. 6: Pendulum free response data, showing the experimental results against the nonlinear friction simulation.

TABLE II: Cart's nonlinear friction parameters

| Parameter | Symbol | Value | Units in SI |
|---|---------------|---------|---|
| Positive cart velocity ($\dot{x}_c > 0$) | | | |
| viscous friction coefficient | $f_{v,c}^+$ | 5.6864 | $\text{N} \cdot \text{s} \cdot \text{m}^{-1}$ |
| Coulomb friction | $F_{c,c}^+$ | 1.8 | N |
| static friction | $F_{brk,c}^+$ | 5.5968 | N |
| Stribeck velocity coefficient | $c_{v,c}^+$ | 100 | $\text{s} \cdot \text{m}^{-1}$ |
| Negative cart velocity ($\dot{x}_c < 0$) | | | |
| viscous friction coefficient | $f_{v,c}^-$ | 6.1403 | $\text{N} \cdot \text{s} \cdot \text{m}^{-1}$ |
| Coulomb friction | $F_{c,c}^-$ | 1.79852 | N |
| static friction | $F_{brk,c}^-$ | 6.4246 | N |
| Stribeck velocity coefficient | $c_{v,c}^-$ | 100 | $\text{s} \cdot \text{m}^{-1}$ |
| cart linearised friction coefficient | b | 5.91 | $\text{N} \cdot \text{s} \cdot \text{m}^{-1}$ |

TABLE III: Pendulum's nonlinear friction parameters

| Parameter | Symbol | Value | Units in SI |
|--|-------------|------------------------|---|
| viscous friction coefficient | $f_{v,p}$ | 3.5×10^{-4} | $\text{N} \cdot \text{s} \cdot \text{rad}^{-1}$ |
| Coulomb friction | $F_{c,p}$ | 6.9×10^{-4} | N |
| static friction | $F_{brk,p}$ | 8×10^{-4} | N |
| Stribeck velocity coefficient | $c_{v,p}$ | 50 | $\text{s} \cdot \text{rad}^{-1}$ |
| pendulum linearised friction coefficient | k | 3.507×10^{-4} | $\text{N} \cdot \text{s} \cdot \text{rad}^{-1}$ |

response test was performed. The pendulum rod was released from an initial angle, and the system's motion was recorded until the rod came to a stand-still. The pendulum's nonlinear friction parameters were identified by fitting experimental data from multiple such runs to the generic friction model (3), with the obtained numerical values summarized in Table III. As indicated in Fig. 6, the thus specified friction model allows for a very good agreement between the simulation results and the experimental data. It is also noted that the model can also accurately predict the, essentially negligible, motion of the cart during this experiment, providing further validation for the identified values of the cart's friction parameters.

D. Virtual model of the cart-pendulum system

As a complementary educational tool, a virtual model of the cart-pendulum system was developed in Simulink. This integrates the system's full nonlinear motion equations with a visualization module based on a CAD model of the physical platform. The virtual model allows for students to familiarize with the system and design different control strategies for various operation scenarios in a safe and convenient manner, prior to implementation on the physical hardware.

IV. CONTROL DESIGN

The system's nonlinear equations of motion exhibit two equilibria in relation to the angular position of the rotating rod, namely a stable equilibrium for $\theta = 0$ (pendulum hanging downwards) and an unstable one for $\theta = \pi$ (pendulum upright). Linear feedback control laws can be designed to regulate the pendulum's angular position in these equilibria using of a linearised state-space model of the system, whose derivation is presented below.

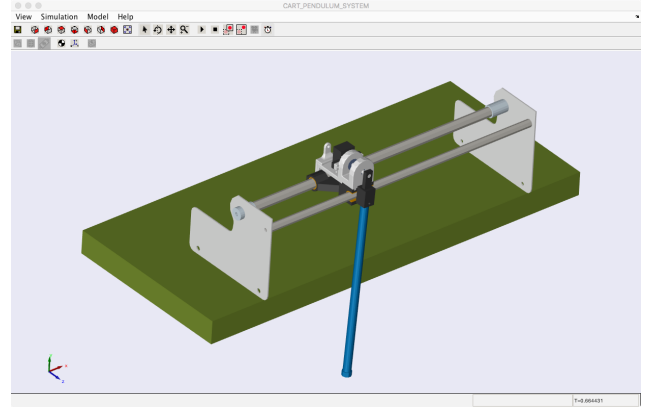


Fig. 7: Visualization of the physical cart-model platform in Simulink.

A. Model linearisation

The linearisation process is hindered by the friction force terms that appear in (1) and (2), due to the presence of $\text{sgn}(v)$ in (3). Therefore, a linear approximation of (3) with a first-order polynomial was taken, converting to $b\dot{x}_c$ and $k\dot{\theta}$ the friction for the cart and pendulum, respectively (see Tables II and III for their numerical values).

Defining the system's state vector as $\mathbf{x} = [x_c \ \dot{x}_c \ \theta \ \dot{\theta}]^T$, the stable equilibrium point corresponds to $\bar{\mathbf{x}} = [* \ 0 \ 0 \ 0]^T$ with an associated control input force of $\bar{F} = 0$. In this case (gantry crane configuration), the linearised state-space description of the system, obtained through Jacobian linearisation, becomes:

$$\dot{\mathbf{x}} = \mathbf{A}\mathbf{x} + \mathbf{B}u \quad (8)$$

$$\mathbf{y} = \mathbf{C}\mathbf{x} \quad (9)$$

where, denoting as $q = (m_c + m_p)I_p + m_c m_p \ell^2$:

$$\mathbf{A} = \begin{bmatrix} 0 & 1 & 0 & 0 \\ 0 & \frac{-(I_p + m_p \ell^2)}{q} b & \frac{m_p^2 \ell^2}{q} g & \frac{m_p \ell}{q} k \\ 0 & 0 & 0 & 1 \\ 0 & \frac{m_p \ell}{q} b & \frac{-(m_c + m_p) m_p \ell}{q} g & \frac{-(m_c + m_p) k}{q} \end{bmatrix}$$

$$\mathbf{B} = \begin{bmatrix} 0 \\ \frac{(I_p + m_p \ell^2)}{q} \\ 0 \\ \frac{-m_p \ell}{q} \end{bmatrix}, \quad \mathbf{C} = \begin{bmatrix} 1 & 0 & 0 & 0 \\ 0 & 0 & 1 & 0 \end{bmatrix} \quad (10)$$

Here, \mathbf{A} , \mathbf{B} , and \mathbf{C} respectively denote the system, input, and output matrices, $u = F$ is the control input (applied force) and \mathbf{y} the output vector.

For the linearisation in the upright position (inverted pendulum configuration), instead of the angle θ , it is convenient to use as state variable the angular deviation $\phi = \theta - \pi$ of the pendulum from the upper vertical position. In this case, noting that $\dot{\phi} = \dot{\theta}$ and $\ddot{\phi} = \ddot{\theta}$, the state variable vector becomes $\mathbf{x} = [x_c \ \dot{x}_c \ \phi \ \dot{\phi}]^T$. Linearization about the equilibrium point of $\bar{\mathbf{x}} = [* \ 0 \ 0 \ 0]^T$ and $\bar{F} = 0$, then eventually yields the following state-space matrices:

2) *Velocity estimation*: The linear controllers of Section IV-B require that all four state variables in \mathbf{x} are available for use in the feedback laws. However, this is not directly the case for the physical platform, since the incremental encoders measure the positions x_c and θ . This necessitates an online estimation of \dot{x}_c and $\dot{\theta}$ from the position measurements, here derived via the method of *algebraic derivative estimation* [11]. Following this method, the pendulum's angular velocity was obtained by the following integral:

$$\dot{\theta} = \frac{1}{T^3} \int_0^T (6\tau - 12T)\theta(t - \tau) d\tau \quad (21)$$

Selecting an integration window of $T = 15$ ms, the above expression was implemented as a finite impulse response (FIR) digital filter with a sampling time of 0.5 ms. The same approach was employed for the cart velocity estimation. Overall, the algebraic method of velocity estimation with the above parameter values improved considerably the performance of the system with regard to noise suppression.

B. Pole placement design

Typically, in pole placement designs the desired eigenvalues of the closed-loop system for full state feedback are specified so that the system's behaviour is determined by dominant poles. According to this approach, two of the cart-pendulum system's eigenvalues are defined as dominant conjugate complex poles, placing the other three poles on the real axis at a sufficient distance from the complex pole pair. Thus, considering the closed-loop system of Fig. 8, the desired 5th order characteristic polynomial will be of the following format:

$$(s - p_3)(s - p_4)(s - p_5)(s^2 + 2\zeta\omega_n s + \omega_n^2) \quad (22)$$

where ζ the damping coefficient and ω_n the natural frequency associated with the desired dominant complex poles, i.e.:

$$p_{1,2} = -\zeta\omega_n \pm \left(\omega_n\sqrt{1 - \zeta^2}\right) i \quad (23)$$

The three real poles are then selected so that they lie further away from $p_{1,2}$ (i.e., $p_j \gg -\zeta\omega_n$, $j = 3, 4, 5$) in order to avoid adversely affecting the closed-loop response, while also taking into account control input limitations. To demonstrate this method, we consider here the gantry crane configuration of the cart-pendulum system through the linearised dynamics of (8)-(10) and design using pole placement an augmented state feedback controller to allow for cart position control with suppressed pendulum oscillations. As a first step, utilizing Matlab's `ctrb`, `rank` functions, we confirm that the controllability matrix (17) has $\text{rank}(\mathbf{G}) = 5$, i.e., the system meets the full controllability criterion. Subsequently, we specify a desired settling time of $t_s = 2.0$ s with a 2% maximum overshoot, yielding a corresponding damping coefficient $\zeta = 0.78$ and natural frequency $\omega_n \approx 4/(\zeta t_s) = 2.565$ rad/s for the desired complex conjugate eigenvalues. The remaining three real poles are then selected after some experimentation with the simulation model. Using Matlab's `place` function, the thus specified desired eigenvalues $\{-6, -13, -14, -2 \pm 1.6i\}$

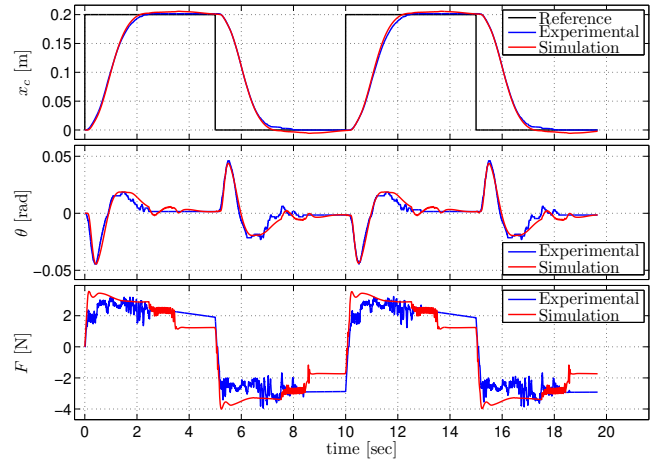


Fig. 9: Experimental results for the control of the cart-pendulum system in the gantry crane configuration, shown against simulations with the full nonlinear model of the system.

of the feedback system matrix $\mathbf{A}_1 - \mathbf{B}_1\mathbf{K}$, yielded the following gain vector \mathbf{K} :

$$\mathbf{K} = [134.67 \quad 45.15 \quad -55.60 \quad 4.09 \quad -146.18]$$

Experimental results for the system's response under this controller, involving a square-wave reference cart position signal, are shown in Fig. 9, along with equivalent simulation results. It can be seen that the cart tracks the desired position with a settling time of about 2 s and minimal steady-state error, while the pendulum deviates less than 0.05 rad from its equilibrium, exhibiting the same settling time as the cart. Moreover, it is noted that the simulation accurately predicts the system's response, thus highlighting its effectiveness as a control design tool.

C. Linear quadratic regulator design

The LQR design yields an optimal controller that minimizes the following infinite horizon quadratic cost function:

$$J = \int_0^\infty (\mathbf{x}^\top \mathbf{Q} \mathbf{x} + \mathbf{u}^\top \mathbf{R} \mathbf{u}) dt \quad (24)$$

where \mathbf{Q} and \mathbf{R} are symmetric positive-definite cost matrices, respectively associated with the system state errors and the control effort. Most often, \mathbf{Q} and \mathbf{R} are defined as positive diagonal matrices, where the Q_{ii} elements penalize the relative error in individual state variables, while R_{ii} elements penalize actions in u_i . For (8), the optimized gain values in the feedback law $\mathbf{u} = -\mathbf{K}\mathbf{x}$ are derived from:

$$\mathbf{K} = \mathbf{R}^{-1} \mathbf{B}^\top \mathbf{P} \quad (25)$$

where \mathbf{P} is found by the solution of the Riccati algebraic equation:

$$\mathbf{A}^\top \mathbf{P} + \mathbf{P} \mathbf{A} - \mathbf{P} \mathbf{B} \mathbf{R}^{-1} \mathbf{B}^\top \mathbf{P} + \mathbf{Q} = 0 \quad (26)$$

Alternatively, one can use Matlab's `lqr` function, which conveniently calculates \mathbf{K} given the \mathbf{A} , \mathbf{B} , and \mathbf{Q} , \mathbf{R} matrices.

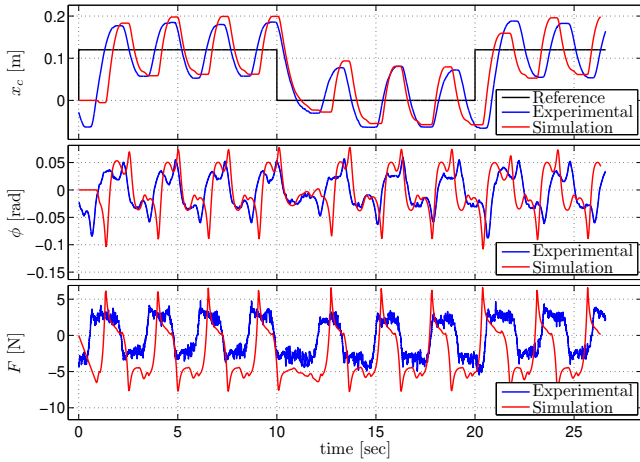


Fig. 10: Experimental results for the control of the cart-pendulum system in the inverted pendulum configuration, shown against simulations with the full nonlinear model of the system.

Here, LQR is employed to design a controller that stabilizes the pendulum in its inverted configuration, whilst tracking a desired cart position, as per Fig. 8. Considering the state space formulation (16) with the corresponding linearised dynamics of (11), it can be confirmed that the $(\mathbf{A}_1, \mathbf{B}_1)$ pair, as for the gantry configuration, exhibits the property of full controllability. Using Matlab's `lqr` function, for $\mathbf{Q} = \text{diag}\{200, 0, 500, 0, 1300\}$ and $\mathbf{R} = [0.35]$, the optimum feedback gain values are then calculated as:

$$\mathbf{K} = \begin{bmatrix} -67.25 & -38.33 & 95.73 & 13.07 & 60.94 \end{bmatrix}$$

The eigenvalues of the closed loop system matrix $\mathbf{A}_1 - \mathbf{B}_1 \mathbf{K}$ are then found to be $\{-11.7 \pm 8.3i, -1.8 \pm 1.9i, -2.1\}$, confirming the system's stability. Note that the LQR design yields one real and two pairs of complex eigenvalues.

The experimental results, shown in Fig. 10, indicate that the controller is effective in stabilizing the pendulum, while tracking the desired cart position square-wave signal. As is often the case with practical implementations of the inverted pendulum system, the cart response exhibits a steady-state oscillation of about ± 5 cm, mainly attributed to the non-linear effects of friction. The maximum pendulum deviation from its equilibrium position is less than 0.04 rad for this experiment. Regarding the simulation results, it can be seen that, although not perfect, the model successfully captures all main characteristics of the system's response also in this case.

Finally, Fig. 11 presents experimental results demonstrating how the LQR controller effectively counteracts external disturbances (introduced by manually tapping the rod) during balancing of the inverted pendulum.

VI. CONCLUSIONS

We have presented a cart-pendulum plant offering performance and robustness directly comparable to that of commercially available units, while being considerably more affordable. The physical plant is complemented by a virtual model to

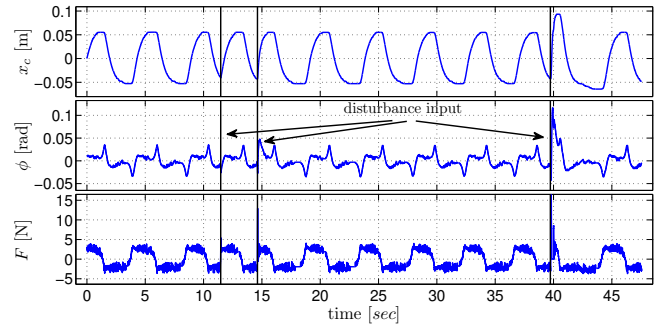


Fig. 11: Experimental results demonstrating the rejection of external disturbances during balancing in the inverted pendulum configuration.

provide a complete and versatile platform for demonstrating, teaching, and investigating control-related topics of varying degrees of complexity. This was demonstrated via experiments and corresponding simulations for two different designs of an augmented state feedback scheme, to allow cart positioning while minimizing pendulum deviations from its equilibrium for both the gantry crane and the inverted pendulum configurations. Although not presented here, the swingup manoeuvre has also been successfully implemented on this platform.

The developed cart-pendulum has been successfully employed as an engaging teaching aid in the context of several undergraduate and postgraduate courses taught at the Technological Educational Institute of Crete (Greece), related to dynamics, control, embedded systems and robotics. Future work will involve integration of this platform in a remote laboratory setup.

REFERENCES

- [1] K. Pathak, J. Franch, and S. K. Agrawal, "Velocity and position control of a wheeled inverted pendulum by partial feedback linearization," *IEEE Transactions on Robotics*, vol. 21, no. 3, pp. 505–513, 2005.
- [2] S. C. Peters, J. E. Bobrow, and K. Iagnemma, "Stabilizing a vehicle near rollover: An analogy to cart-pole stabilization," in *IEEE Int. Conf. on Robotics and Automation (ICRA)*, 2010, pp. 5194–5200.
- [3] T. Komura, A. Nagano, H. Leung, and Y. Shinagawa, "Simulating pathological gait using the enhanced linear inverted pendulum model," *IEEE Transactions on Biomedical Engineering*, vol. 52, no. 9, pp. 1502–1513, 2005.
- [4] H. T. Teixeira, V. S. de Mattos Siqueira, and C. J. Munaro, "Comparison of methods for estimation and compensation of friction applied to an inverted pendulum," in *IEEE Int. Conf. on Control and Automation (ICCA)*, 2011, pp. 818–823.
- [5] Quanser Inc., "Linear servo base unit with inverted pendulum," available online at <https://www.quanser.com/products/linear-servo-base-unit-inverted-pendulum/>.
- [6] Inteco, "Pendulum & cart control system," available online at <http://www.inteco.com.pl/products/pendulum-cart-control-system/>.
- [7] Bytronic Ltd., "Pendulum control system," available online at <http://www.bytronic.net/product/pendulum-control-system/>.
- [8] E. Kourtikakis, E. Kapellakis, J. Fasoulas, and M. Sfakiotakis, "An embedded controller for the pendubot," in *Int. Symp. on Ambient Intelligence and Embedded Systems (AmiEs16)*, 2016.
- [9] H. Olsson, K. Åström, C. de Wit, M. Gäfvert, and P. Lischinsky, "Friction models and friction compensation," *European Journal of Control*, vol. 29, no. 4, pp. 176–195, 1998.
- [10] P. I. Corke, "In situ measurement of motor electrical constants," *Robotica*, vol. 14, no. 4, pp. 433–436, 1996.
- [11] M. Mboup, C. Join, and M. Fliess, "A revised look at numerical differentiation with an application to nonlinear feedback control," in *IEEE Medit. Conf. on Control and Automation (MED)*, 2007, pp. 1–6.